PROCEEDINGS OF SPIE

SPIEDigitalLibrary.org/conference-proceedings-of-spie

Real-time monitoring system for multi-MW scale wind blades using FBG sensors

Hongwei Liu, Zhichun Zhang, Hongbo Jia, Denggang Zhang, Yanju Liu, et al.

Hongwei Liu, Zhichun Zhang, Hongbo Jia, Denggang Zhang, Yanju Liu, Jinsong Leng, "Real-time monitoring system for multi-MW scale wind blades using FBG sensors," Proc. SPIE 10972, Health Monitoring of Structural and Biological Systems XIII, 109721O (1 April 2019); doi: 10.1117/12.2514675

SPIE.

Event: SPIE Smart Structures + Nondestructive Evaluation, 2019, Denver, Colorado, United States

Real-time monitoring system for multi-MW scale wind blades using FBG sensors

Hongwei Liu [a], Zhichun Zhang [a], Hongbo Jia [a], Denggang Zhang[b], Yanju Liu[c], Jinsong Leng*[a]

[a]National Key Laboratory of Science and Technology on Advance Composites in Special Enviroments, Harbin Institute of Technology, Harbin 150080, China; [b]C-9th Floor, Tower B Zone 6, Zhongguancun Dongsheng Technology Park, No.66 Xixiaokou Road, Haidian District, Beijing, 100192, China; [c]Department of Astronautical Science and Mechanics, Harbin Institute of Technology, Harbin 150080, China;

ABSTRACT

Measured by distributed fiber Bragg grating (FBG) sensors, an application and strain analysis of real-time structural health monitoring system for muti-MW scale wind blades during the service process has been established and investigated. The experiments of the multi-MW scale wind turbine were performed at the top of the hill, near the sea and the FBG sensors were mounted at various locations on the internal surfaces of the rotating blades. The feasibility and effectiveness of the system were validated by continuously transmitting the optical signals between the FBG demodulator and the sensors. The internal dynamic strain of the blades during the environmental fatigue loadings were monitored, valuated and given crash alert with FBG sensors through the results of preliminary field tests. Through Hilbert-Huang transform (HHT), the strain data were decomposed into a series of intrinsic mode functions (IMF) and residual component by the empirical mode decomposition (EMD) method under different frequencies.

Keywords: FBG, structural health monitoring, wind blade, Hilbert-Huang transform

1. INTRODUCTION

Due to the high cost of limited energy, the global energy crisis is focusing much attention on clean and renewable energy. Renewable Energy Policy Network for the 21st Century (REN21) released Renewables 2017 Global Status Report to emphasize the importance of clean and renewable energy and pointed that more than 24 countries met 5% or more of their annual electricity demand through wind power in 2016. In the next 10 years, the offshore and onshore wind power generation cost will fall by 35% and 35% respectively[1]. Wind blades as one of the key components to generate the power in wind turbines exposed to direct harsh environment can be damaged by fatigue fracture, gusts, lightning strikes or humidity changes, erosion and corrosion. In 2015, wind blades are failing at a rate of 0.54% of the global operating blades in worldwide range[2].

To gain enough power, improve safety, minimize the maintenance cost and lower the sudden breakdowns, the wind blades need to be monitored at real-time[3]. With the addition of the sea-land breeze, mountain-valley breeze and other environmental loadings, the structural health monitoring for wind blades during the service process is essential to blade manufacturers and wind farms to improve blade efficiency, enhance the protection of the blades.

Capable of detecting deformation and damage, a large quantity of inspection methods are appropriate for composite materials and structures. While a limited number of inspection methods can be applied to the large wind blades for continuous online monitoring, such as acoustic emission and strain monitoring[4]. Compared with electrical sensors, fiber Bragg grating (FBG) sensors have unique advantages such as immunity from electro-magnetic interference, small size, light weight, corrosion resistance, long term durability and stability, making them increasingly applied in aerospace, civil engineering and other fields[5]. Hence, the development of wind turbine structural health monitoring (SHM) technology using FBG sensors has attracted wide angle attention on renewable energy.

Based on FBG sensors, much effort has been made in wind power field recently as reported in literature. For large wind turbine support structure, Hyung et al. studied the shape estimation of 70 m height wind turbine tower under dynamic loads by FBG sensors[6]. Magdalena and Wiesław investigated the natural frequencies of the support structure in water under wave and rotor excitation by frequency domain decomposition method through FBG sensors[7]. However, the

Health Monitoring of Structural and Biological Systems XIII, edited by Paul Fromme, Proc. of SPIE Vol. 10972, 109721O · © 2019 SPIE
CCC code: 0277-786X/19/$18 · doi: 10.1117/12.2514675

research on structural health monitoring of wind blades is lack of using in service despite a few attempts in laboratory as well as in finite element simulation. Shin et al. investigated the effect of sensor layout on detection capability of a retired 22 m long wind blade and discussed the signals resulting from impacts at different positions[8]. Chen et al. used FBG sensors with a fiber optic rotary joint to monitor a small turbine blade and compared the measured data with IMote2-based wireless strain sensors[9]. Kim et al. studied a bench test of the wind turbine blade by FBG sensors to determine the loading location, magnitude and direction of the imposed loads in the laboratory[10]. Arsenault et al. tested wind turbine blades under rotating conditions by FBG sensors and analyzed the strain data through operational modal analysis (OMA) methods to capture natural frequencies and corresponding mode shapes[11]. Taking into account material failure and property degradation, Chen et al. predict the multiple failure modes and gained the failure mechanisms of the blade by a finite element simulation using a global-local modeling approach and progressive failure analysis (PFA) techniques[12]. In addition, many researchers also paid attention to the data driven approaches on wind blade[13-15], such as operational modal analysis, best-first tree algorithm.

Due to the strong randomness of wind load and the non-linear power system, the large wind blades should be both supervised in time-domain and analyzed in frequency-domain. Moreover, the variation of frequency with time often reveals the rotational frequency of the blade, normal or abnormal, continuous or intermittent, which significantly influences the judgment of maintenance.

The main objective of this paper was to investigate the FBG monitoring system for 42.2-meter wind blades in service. The strain changing was recorded and the instantaneous frequency could be obtained based on Hilbert-Huang transform, aimed at evaluating the change subject to the environmental loadings. Compressive sensing technology is used for signal compression and reconstruction

2. THEORETICAL APPROACH

2.1 FBG sensing principle

FBG sensors are usually fabricated by ultraviolet (UV) laser and the phase mask is a periodic perturbation of the reflective index with a grating structure along a single-mode optical fiber. The measurement principle is to detect the back-reflected wavelength shift produced by the periodic index modulated structure, as shown in Figure 1. The Bragg wavelength of light reflected is defined as：

$$\lambda_B = 2n_{eff}\Lambda \qquad (1)$$

where λ_B is the reflected Bragg wavelength of FBG, n_{eff} is the effective refractive index of the fiber core and Λ is the period of the grating.

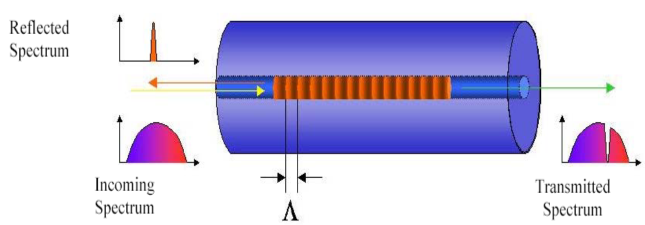

Figure 1 Schematic representation of the FBG working principle

As illustrated in Eq. (1), the Bragg wavelength is a function of the effective refractive index and the period of the grating. According to the researches before, the basic principle of FBG is to monitor the reflected wavelength shift due to changes of the effective refractive index and the grating period result from the strain and temperature, which can be described as:

$$\Delta\lambda = \left(\alpha_f + \xi\right)\lambda_B \Delta T + \left(1 - P_e\right)\lambda_B \varepsilon \qquad (2)$$

where α_f is the thermal-expansion coefficient of the fiber glass, ξ is the thermal-optic coefficient of the fiber glass, ΔT is the temperature change, P_e is the effective photo-elastic coefficient of the fiber glass and ε is the axial strain acted on the FBG.

The typical strain sensitivity of an FBG at 1550 nm is 1.2 pm/$\mu\varepsilon$.

2.2 Hilbert-Huang transform

Proposed by Norden E. Huang, Hilbert-Huang transform (HHT) mainly contains empirical mode decomposition (EMD) method and Hilbert spectrum analysis. Similar to wavelet decomposition, the original signals are decomposed into a number of intrinsic mode functions (IMF) and residual component by EMD method under different frequencies. The instantaneous spectrum of each IMF can be obtained through Hilbert transform. The overall HHT transformation framework is shown in Fig.2.

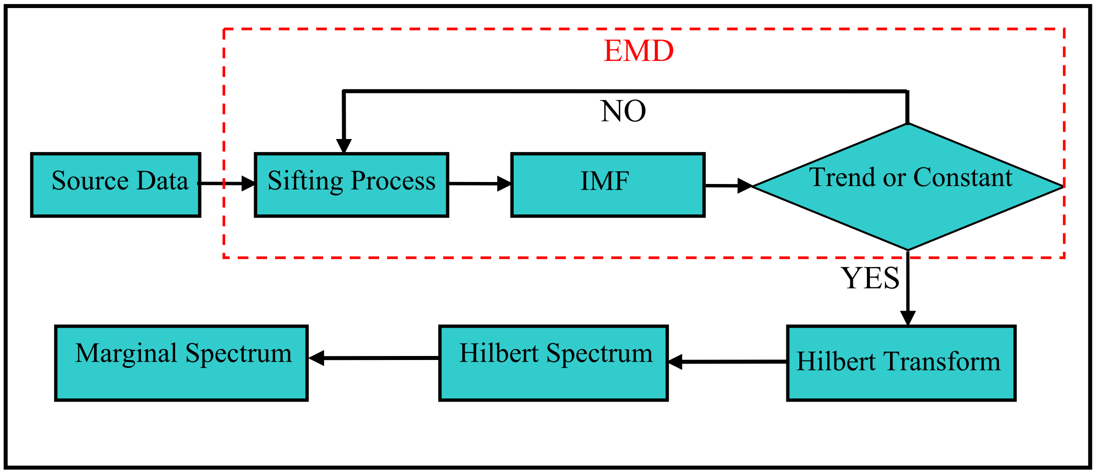

Figure 2 HHT transformation framework

The EMD equation can be expressed as

$$x(t)=\sum_{i=1}^{m}c_i(t)+r(t) \qquad (3)$$

where $c_i(t)$ stands for the each IMF component and $r(t)$ stands for the residual component.

Then the instantaneous frequencies of each IMF component can be obtained by Hilbert transform as follows

$$\tilde{c}_i(t)=\frac{1}{\pi}\int_{-\infty}^{+\infty}\frac{c_i(\tau)}{t-\tau}d\tau \qquad (4)$$

Introducing the analytic signal $z_i(t)$, which is the complex signal of $\tilde{c}_i(t)$, can be defined as

$$z_i(t)=c_i(t)+j\tilde{c}_i(t)=a_i(t)e^{j\phi_i(t)} \qquad (5)$$

where $a_i(t)$ and stand for the amplitude and the phase of instantaneous frequency through Hilbert transform respectively, expressed as

$$a_i(t)=\sqrt{c_i^2(t)+\tilde{c}_i^2(t)} \qquad (6)$$

$$\phi_i(t)=\arctan\left(\frac{\tilde{c}_i(t)}{c_i(t)}\right) \qquad (7)$$

The instantaneous frequency is

$$f_i(t)=\frac{1}{2\pi}\omega_i(t)=\frac{1}{2\pi}\frac{d\phi_i(t)}{dt} \qquad (8)$$

Then Hilbert spectrum $x(t)$ can be expressed as

$$x(t) = \mathrm{Re}\sum_{i=1}^{n} a_i(t) e^{j\phi_i(t)} = \mathrm{Re}\sum_{i=1}^{n} a_i(t) e^{j\int \omega_i dt} \quad (9)$$

where Re stands for real part.

$$H(\omega,t) = x(t) = \mathrm{Re}\sum_{i=1}^{n} a_i(t) e^{j\int \omega_i dt} \quad (10)$$

Integrating with respect to X in terms of time, the marginal spectrum is written as

$$h(\omega) = \int_0^T H(\omega,t) dt \quad (11)$$

where T is the total length of the signal. Hilbert spectrum $H(\omega,t)$ accurately reflects the amplitude of the signal with the change of time during the whole frequency band. Marginal spectrum $h(\omega)$ reflects the amplitude of the signal with the change of frequency during the whole frequency band.

3. STRUCTURAL HEALTH MONITORING SYSTEM

3.1 The monitoring system of wind blades

As a rotating mechanical system, it is essential to transmit the sensors' signal on the rotating blades to the stationary wind turbine. In this experiment, a wireless system with FBG sensors was used to monitor the structural strains of wind turbine blades. A FBG demodulator with wavelength division multiplexing (WDM) technology for data acquisition was installed on the wind turbine hub and the optical signals from FBG sensors arrays mounted on the blades were demodulated in the demodulator and then transmitted to the first wireless router nearby through wire transmission. The first wireless router also installed on the wind turbine hub received the signal and wirelessly transmitted to the second remote wireless router near the main electric control cabinet at the same time. The computer in the tower foundation got the wavelength signal from the second wireless router through a 80-meter length ethernet cable and gave a real-time display. The overall system diagram was shown in Figure 3.

Figure 3(a) The monitoring system of wind blades

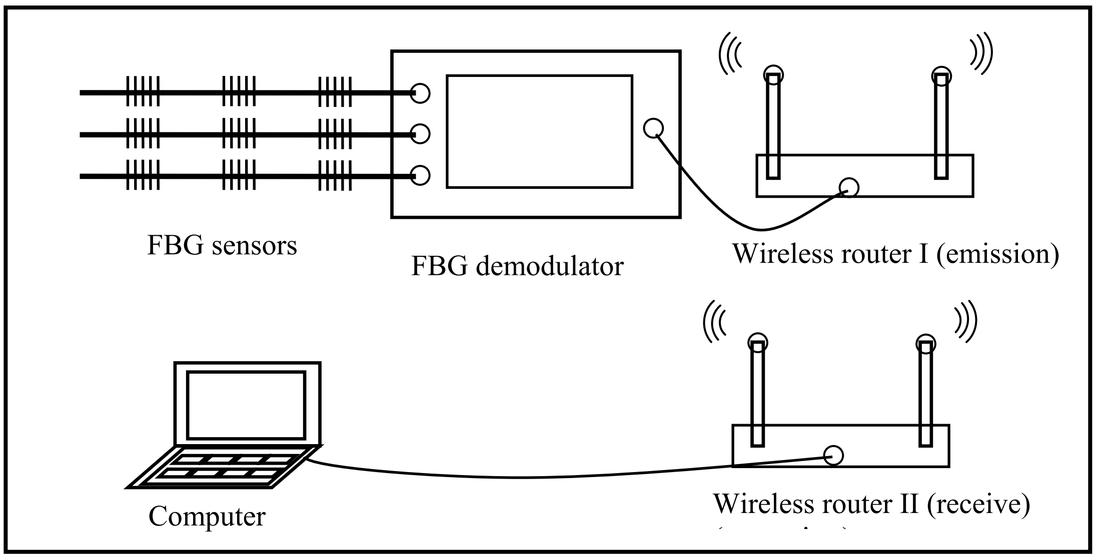

Figure 3(b) The diagram of monitoring system of wind blades

60 FBG sensors were symmetrically installed at the leading edges, trailing edges, webs of the three blades. For convenient comparison, the sensor positions of different blades are consistent, selected at 1.5m, 4m, 6m sections of the blades respectively. FBG temperature sensors were also installed for temperature compensation.

3.2 Results and discussion

Generally, the starting wind speed is required no less than 3m/s. Within a certain period of time, according to the wind speed results measured by the wind field anemometer, the strain results of the blade at different positions under wind load are obtained. The strains at the 6m-leading edge, trailing edge, web of the blade are shown in figure 4. Compared with the strain at leading or trailing edge, the strain at the web of the blade is affected less than them suffered by the wind.

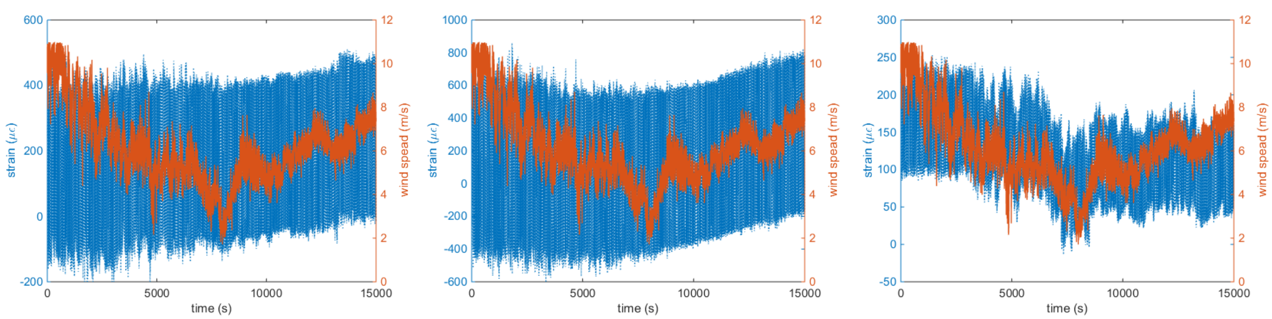

Figure 4(a) strain of 6m-leading edge (b) strain of 6m- trailing edge (c) strain of 6m- web

On account of the wind non-linearity and non-stationarity, Hilbert-Huang transform is an effective method to analyze the strain data of the wind blades. Unlike the Hilbert transform, it avoids the appearance of meaningless negative frequencies by decomposing the signal into a few of components under different scales, namely intrinsic mode functions and residual component. The actual instantaneous frequencies are obtained by each component through Hilbert transform.

Taking the actual data of monitoring point 44 (6m-leading edge -web-center height)in ten minutes into account, the strain data are decomposed into the nine IMF components and a residue as shown in figure 5. It can be seen that the strain data exist a small overall change and a peak at 329.1 second.

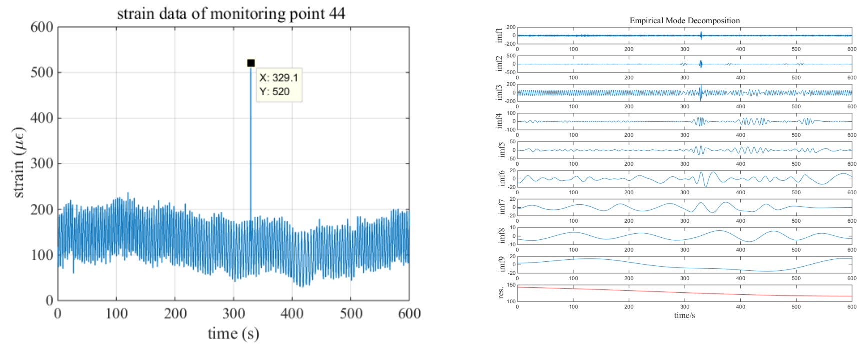

(a) (b)

Figure 5 EMD results of the strain data

According to the Pearson product-moment correlation method, the correlation coefficient can be expressed as:

$$\gamma_{xy} = \frac{n\sum_{i=1}^{n} x_i y_i - \sum_{i=1}^{n} x_i \sum_{i=1}^{n} y_i}{\sqrt{n\sum_{i=1}^{n} x_i^{\ 2} - (\sum_{i=1}^{n} x_i)^2}\sqrt{n\sum_{i=1}^{n} y_i^{\ 2} - (\sum_{i=1}^{n} y_i)^2}} \quad (12)$$

The correlation coefficients of the EMD results between the original strain data are listed in the table 1

Table 1 The correlation coefficients of the EMD results between the original strain data

component	IMF1	IMF2	IMF3	IMF4	IMF5	IMF6	IMF7	IMF8	IMF9	Res
correlation coefficient	0.108	0.209	0.796	0.125	0.046	0.093	0.132	0.069	0.320	0.276

In Table 1, it can be illustrated a good correlation between IMF3 and original data. Combined with Figure 5 the EMD results, the frequency components of the strain data are mainly concentrated in IMF3. Taking an example of IMF3, the instantaneous frequency is obtained through Hilbert transform then.

Figure 6(a) shows the power spectral density (PSD) of IMF3. It is clearly seen that the signal intensity is collected in order of the frequencies and the PSD reaches its maximum at the frequency of 0.2336Hz. In order to analyze the instantaneous frequency of IMF3, the spectrum of IMF3 component has been processed by the Hilbert transformation, as shown in figure 6(b). Combined with figure 5(a) the original strain data, there exists a relative stable frequency over the 10 minutes' time and 4 frequency peaks due to the peak strain signals.

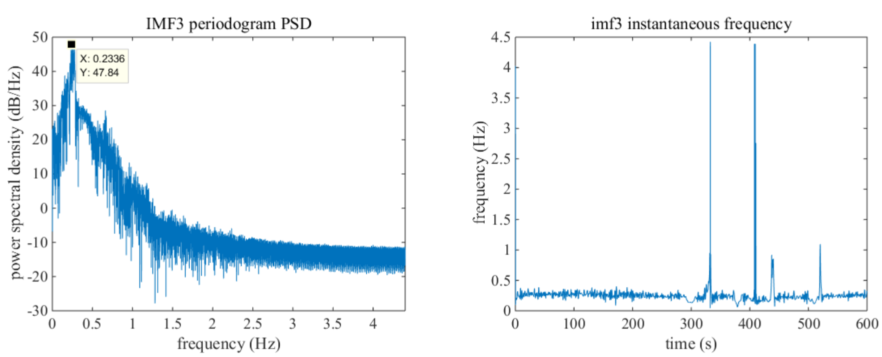

Figure 6(a) PSD of IMF3 (b) the instantaneous frequency of IMF3

Due to the non-stationary and non-linear signal, it's more accurately responsive to the actual frequency components for marginal spectrum than the Fourier spectrum.

Figure 7 illustrates the Hilbert-Huang spectrum of the total 10 minutes' strain data. It can be seen clearly that the amplitude of the data varies with the change of time during the whole frequency band. Compared with figure5(a) the original strain data, there exist a number of frequencies at the time of the peak appearance with higher amplitudes.

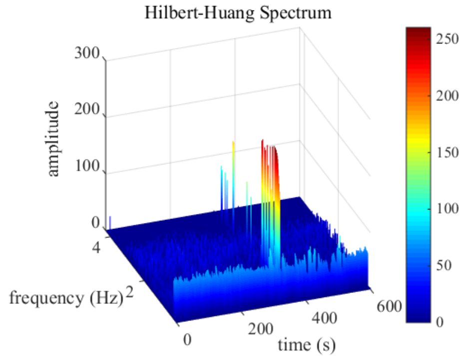

Figure 7 Hilbert-Huang spectrum of the total 10 minutes' strain

Figure 8 shows the marginal spectrum of the total 10 minutes' strain data. It can be seen that the energy amplitude of the data varies with the change of frequency during the whole frequency band. Moreover the amplitude reaches the maximum at the frequency of 0.2447Hz.

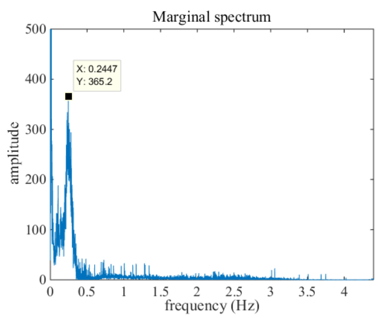

Figure 8 The marginal spectrum of the strain data

In order to reduce the storage of data, compressive sensing technology is applied and can greatly reduce the data volume for remote transmission and reception. Compressive Sensing recover the signal from small set of available samples. After discrete cosine transform (DCT) conversion, the strain signal becomes sparse and it can be further sparse through a threshold to reduce the data.

Figure 9 shows the compressive sensing of the strain data, DCT signal and DCT reconstruction signal.

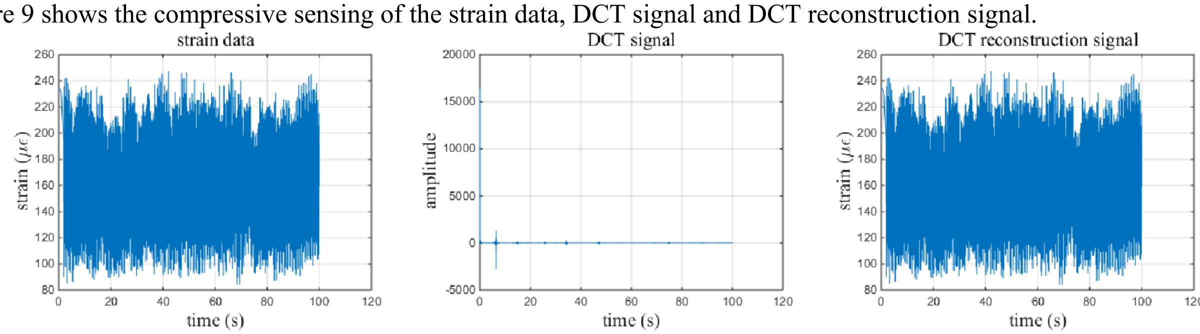

Figure 9 the compressive sensing

4. CONCLUSIONS

In this paper, a real-time monitoring system using the FBG sensors has been applied to the operational condition of a multi-MW scale wind turbine blade. The feasibility and effectiveness of the system are validated and the strain data recorded by the computer have shown that the proposed system has a stable, accurate performance and potential ability in the field of the structural monitoring of wind blades during service process. The analytical strain model based on the HHT is decomposed by the EMD into several IMF components, different forecast methods may be established respectively according to their frequency of the spectrum of each component. In order to reduce the storage of data, compressive sensing technology can greatly reduce the data volume for remote transmission and reception.

ACKNOWLEDGEMENT

This work is supported by the Foundation for Innovative Research Groups of the National Nature Science Foundation of China (Grant No. 11421091) and Special Funds for Scientific and Technological Innovation Talents of Harbin (Grant No. JJ20170379).

REFERENCES

[1] REN 21 Steering Committee, "Renewables 2017 global status report", Report, Renewable Energy Policy Network for the 21st Century (2017).
[2] Campbell S., "Annual blade failures estimated at around 3800", Wind Power Monthly, 14 May (2015).
[3] Huh Y., Kim J. and Hong S., "Response of impedance measured by polyvinylidene fluoride film sensors to damage propagation for wind turbine blade", Journal of Intelligent Material Systems and Structures, 25(5), 606-612 (2014).
[4] Schubel P. J., Crossley R. J., Boateng E. K. G. and Hutchinson J. R., "Review of structural health and cure monitoring techniques for large wind turbine blades", Renewable Energy 51, 113-123 (2013).
[5] Kouroussis G., Caucheteur C., Kinet D., Alexandrou G., Verlinden O., Moeyaert V., "Review of trackside monitoring solutions: from strain gages to optical fibre sensors", Sensors, 15, 20115-20139 (2015).
[6] Bang H. J., Ko S. W., Jang M. S. and Kim H. I., "Shape estimation and health monitoring of wind turbine tower using a FBG sensor array", IEEE Instrumentation & Measurement Technology Conference, 8443(8), 496-500 (2012).
[7] Mieloszyk M., Ostachowicz W., "An application of structural health monitoring system based on FBG sensors to offshore wind turbine support structure model", Marine Structures, 51, 65-86 (2017).
[8] Shin C. S., Chen B. L., Cheng J. R. and Liaw S. K., "Impact Response of a Wind Turbine Blade Measured by Distributed FBG Sensors", Materials and Manufacturing Processes, 25, 4, 268-271 (2010).
[9] Chen Y., Ni Y. Q., Ye X. W., Yang H. X. and Zhu S., "Structural health monitoring of wind turbine blade using fiber Bragg grating sensors and fiber optic rotary joint", Proc. SPIE 8345 (2012).
[10] Kim C., Kim K., Kim H., Paek I., Yoo N., Nam Y., Campagnolo F. and Bottasso. C, "A method to estimate bending moments acting on a wind turbine blade specimen using FBG sensors" International Journal of Precision Engineering and Manufacturing, 13(7), 1247-1250 (2012).
[11] Arsenault T. J., Achuthan A., Marzocca P., Grappasonni C. and Coppotelli G., "Development of a FBG based distributed strain sensor system for wind turbine structural health monitoring", Smart Materials and Structures, 22(11), 075027 (2013).
[12] Chen X., Zhao W., Zhao X. L. and Xu J. Z., "Failure test and finite element simulation of a large wind turbine composite blade under static loading", Energies, 7, 2274-2297 (2014).
[13] Joshuva. A., Sugumaran. V., "A data driven approach for condition monitoring of wind turbine blade using vibration signals through best-first tree algorithm and functional trees algorithm: A comparative study", ISA Transactions, 67, 160-172 (2017).
[14] Kim H. I., Han J. H. and Bang H. J., "Real-time deformed shape estimation of a wind turbine blade using distributed fiber Bragg grating sensors", Wind Energy, 7, 1455-1467 (2014).
[15] Yang W.X., Lang Z.Q. and Tian W.Y., "Condition monitoring and damage location of wind turbine blades by frequency response transmissibility analysis", IEEE Transactions on Industrial Electronics 62(10):1-1 (2015).